Anal. Bioanal. Electrochem., Vol. 12, No. 2, 2020, 263-276

Analytical & Bioanalytical Electrochemistry

Full Paper

Synthesis of Ytterbium Tungstate with Excellent Pseudocapacitive Behavior and a High Cycling Stability Material for Supercapacitors

Hamid Reza Naderi,[1] Ali Sobhani-Nasab[2,3,*] Esmail Sohouli,[4] Kourosh Adib[5] and Ebrahim Naghian[6]

[1]*Novin Ebtekar Company, Exclusive Agent of Metrohm-Autolab and Dropsens Companies, Tehran, Iran*
[2]*Social Determinants of Health (SDH) Research Center, Kashan University of Medical Sciences, Kashan, Iran*
[3]*Core Research Lab, Kashan University of Medical Sciences, Kashan, Iran*
[4]*Young Researchers and Elite Club, Science and Research Branch, Islamic Azad University, Tehran, Iran*
[5]*Department of Chemistry, Imam Hossein University, Tehran, Iran*
[6]*Department of Chemistry, South Tehran Branch Islamic Azad University, Tehran, Iran*

*Corresponding Author, Tel.: +98 9137290874; Fax: +983155316558

E-Mail: Ali.sobhaninasab@gmail.com

Received: 25 November 2019 / Received in revised form: 22 January 2020 / Accepted: 24 January 2020 / Published online: 29 February 2020

Abstract- Nanoparticles of ytterbium tungstate prepared through the direct addition of an Yb^{3+} solution to a tungstate solution, were computed through Fourier transform infrared spectroscopy (FTIR), scanning electron microscopy (SEM), energy-dispersive X-ray spectroscopy (EDS). Further the supercapacitive characteristics of the nanoparticles, as a potential material for constructing electrodes, were evaluated through cyclic voltammetry (CV), galvanostatic charge/discharge (GCD) and electrochemical impedance spectroscopy (EIS). Electrodes made of the $Yb_2(WO_4)_3$ had a specific capacitance (SC) value of 336 F g^{-1} in a 2.0 M H_2SO_4 solution at a potential scan rate of 2 mV s^{-1}; and 298 F g^{-1} at a current density of 1 A g^{-1} based on GCD tests. The electrodes also revealed to have a 95.8% cycling durability after 4000 potential cycles.

Keywords- Ytterbium Tungstate, Nanoparticles, Supercapacitors Precipitation

1. INTRODUCTION

In the last years, novel materials which have been derived from nanomaterials have been received considerable interest. This reasonably refers to their special chemical as well as physical features [1-11]. Of all kinds of nanosized materials, magnetic structures have been much focused because they have morphology- and size- based characteristics [12-21]. Electrochemical capacitors, also known as supercapacitors, are devices in which electrodes made of electroactive materials (e.g., metal tungstate and Ni), produce Faradaic electrosorption or oxidation/reduction currents [22-24]. These energy storage/delivery devices offer great technical potentials due to their high-power, acceptable capacity, and cycle durability.

Supercapacitors have recently gained a considerable amount of interest given their unique properties [25, 26], including their very high capacitance per unit volume and energy density values, as opposed to other capacitors. Although the supercapacitors available have energy densities of about 10% of batteries, they offer 10 to 100 times higher power densities, which means they have shorter charge/discharge cycles than batteries, in addition to their greater endurance when subjected to several charge/discharge cycles [27,28].

The original capacitance of pseudocapacitors is based on electrochemically active compounds through fast faradic redox reaction, and many material have been used in production of pseudocapacitors in recent years [29]. Of all, varying metal oxides have been used as supercapacitor active substances and in this family, binary oxides such as metal tungstates have attracted particular attention. That is why much research has been conducted in this area. Metal tungstate display high supercapacitive efficiency and good functional features including substantial specific capacitance, very great cyclic performance and acceptable rate capability [30,31].

Interestingly, compounds of lanthanide elements offer unique properties due to the contraction resulting from of the filling their 4f orbitals, and also the shielding of the f orbitals by the 5s and 5p shells [32-34]. Various lanthanide tungstate and molybdate salts are known to have attractive properties like very high mechanical strengths and oxide ion conductivity, as well as advantageous thermal and chemical stabilities. On the other hand, ceramics or nano-crystallites of these tungstate or molybdate salts have been reported to enhance the behavior of solid-state lasers, optical fibers, as well as scintillators [35,36].

This paper focused on the fabrication of ytterbium (III) tungstate nanoparticles using a precipitation approach. The composition and shape of the final materials were evaluated through various analytical techniques, as were their supercapacitive qualities by electroanalytical techniques.

2. EXPERIMENTAL

2.1. Materials and physical measurements

Sodium tungstate, and ytterbium(III) chloride of analytical grade purity were obtained from Merck Co., and nanostructured ytterbium(III) tungstate particles were prepared via adding an 0.01 M aqueous solution of Yb^{3+} at 40.0 $mLmin^{-1}$ to a 0.01 M tungstate solution in water under stirring at 30 °C. The resulting precipitate was separated and repeatedly washed with distilled water, and then with absolute ethanol before drying at 80 °C for about 4 h. Finally the sample was calcined in 750 °C in air for 3 h before analysis like SEM, EDS, FT-IR and UV-Vis.

The evaluation of the product morphology and its energy-dispersive analyses were performed on a Philips XL30 SEM instrument. To this end, the sample particles were coated with a gold film using a BAL-TEC SCD005 sputter coater. The microstructural TEM analyses were performed using a Ziess- EM10C scanning electron microscope, after coating the samples on a Cu Mesh 300 carbon-coated grid. FT-IR characterizations were also performed using a Bruck Equinox 55 instrument and the KBr pellet approach.

2.2. Electrochemical evaluations

An electrochemical system is included in a working, a reference and an auxiliary electrode, which was linked to a computer controlled Autolab PGSTAT204 workstation, was used in these evaluations. The major element of the three electrode system was the working electrode, which was prepared by admixing the prepared nanoparticles as the active material, carbon black, graphite, and PTFE at 65:20:10:5 wt, and a small volume of absolute ethanol. The resulting homogeneous slurry was next coated on a 1 cm^2 stainless steel element and pressed up to 10 MPa to form a tablet electrode pad, and then was dried in a vacuum oven at 80 °C for 4 h. The amount of the active material loaded on the electrode was about 3 mg. A 2.0 M H_2SO_4 solution was used as the electrolyte, and a Pt foil and an Ag/AgCl electrode served as the counter and reference electrodes.

The electrochemical tests included cyclic voltammetry (CV), continues cyclic voltammetry (CCV) galvanostatic charge/discharge (GCD), and electrochemical impedance spectroscopy (EIS). The EIS tests were performed at 100 μHz to 100 kHz and open circuit potential (5 mV). The specific capacitance (SC) values were determined using CV data using the following formula [37].

$$SC = \frac{\mathrm{i}}{mv} = \frac{\int_{V_1}^{V_2} i(V)\, dV}{mv\Delta V} \quad (1)$$

dV: voltage difference; v: scan rate (V s^{-1}); m: mass of the electrode material; V_1 and V_2: initial and final voltages (V).

The SC values were also evaluated using the GCD data and the equation as following:

$$SC = \frac{I\Delta t}{\Delta V} \quad (2)$$

I: GCD current (A); Δ*t*: discharge time (s); and V: the potential drop at discharge (V).

3. RESULTS AND DISCUSSION

3.1. Characterization of the nanoparticles

The SEM results obtained for the samples (Fig. 1), indicate the existence of uniform 25-30 nm spherical particles. The TEM results (Fig. 2) further confirmed these observations. The optimal ytterbium(III) tungstate nanomaterials were also characterized through powder XRD to evaluate their chemical composition. The results (Fig. 3) demonstrated that the characteristic XRD pattern of the ytterbium(III) tungstate nanoparticles, including strong main peaks in a relatively smooth baseline which agrees with the hydrated structure of ytterbium(III) tungstate from PC-APD, diffraction software (No.00-028-1290). The purity of the product was further assessed through EDS analyses (Fig. 4), which only indicated the presence of Yb, W and O.

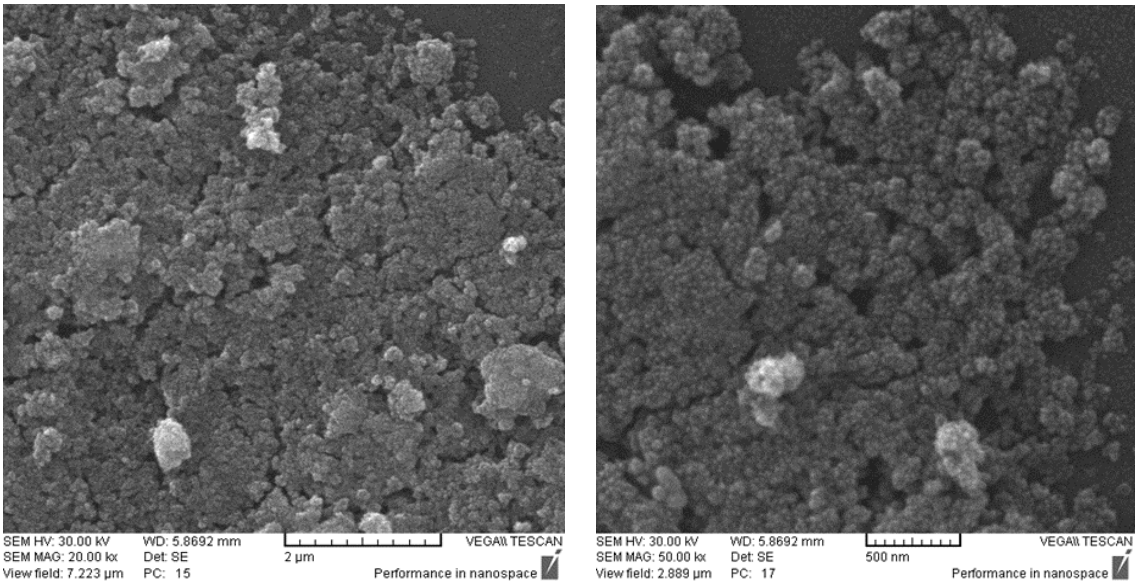

Fig. 1. SEM images of ytterbium tungstate nanoparticles synthesized via chemical precipitation reaction

FT-IR spectra of the samples both before and after thermal treatment at 750 ºC were also recorded. Considering, the untreated sample (Fig. 5a) three wide absorption bands were observed at around 847.6, 1628.6 and 3445.2 cm^{-1}, which were weakened after thermal treatment at 750 °C (Fig. 5b) reflecting the evaporation of surface adsorbed water. Also the

absorption bands corresponding to the scheleete type structure can be seen at 948.9, 860.2, 736.8, 671.2, 486.0 and 466.7 cm^{-1}. The absorption bands at 948.9 and 860.2 cm^{-1} were related to the vibration of the W-O bond. Symmetrical vibrations of the bridging oxygen atoms of the Yb–O–W groups producing absorption band at 736.8 cm^{-1}. The absorption bands at 671.2 and 486.0 cm^{-1} can be due to the of W–O as well as Yb–O bonds [38-40].

UV-Vis spectroscopy analyses were also performed to characterize the absorption behavior of the optimal nanostructures. Based on the results, e.g. Fig. 6 which displays the UV-Vis absorption spectrum of a dispersion of the ytterbium(III) tungstate nanoparticles in water, the main absorption happened at 220 nm. This can be owing to the great quantum confinement of the excitonic transitions in nano-structures, reflects the fine size of the crystals [41].

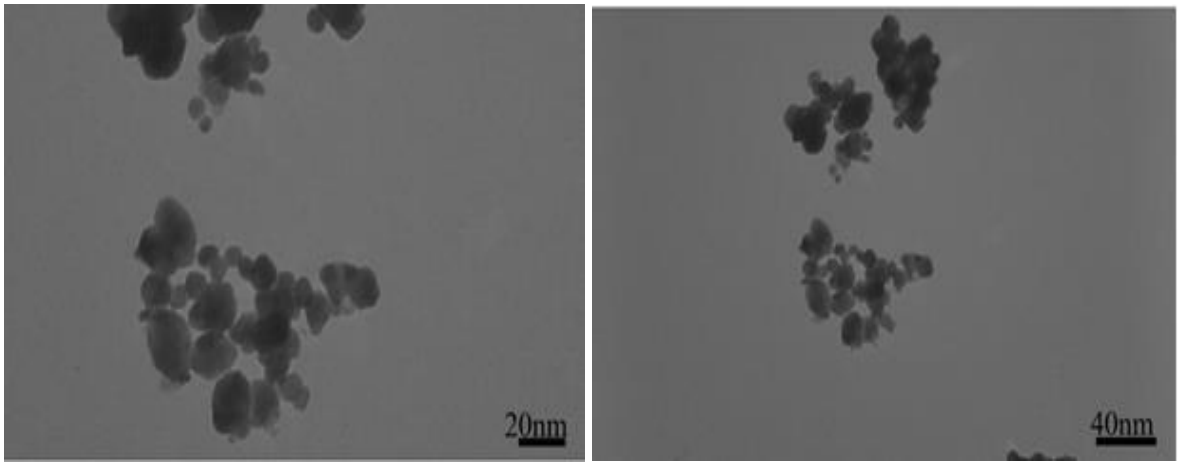

Fig. 2. TEM images of ytterbium tungstate nanoparticles synthesized via chemical precipitation reaction

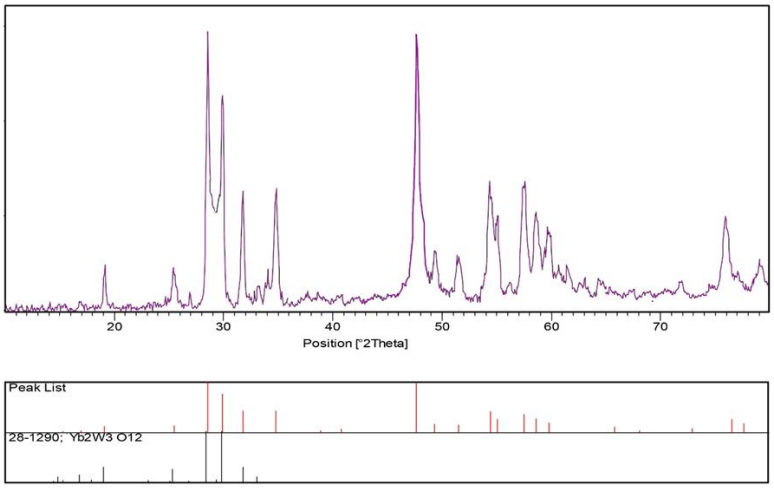

Fig. 3. XRD pattern for synthesized ytterbium tungstate nanoparticles by precipitation reaction

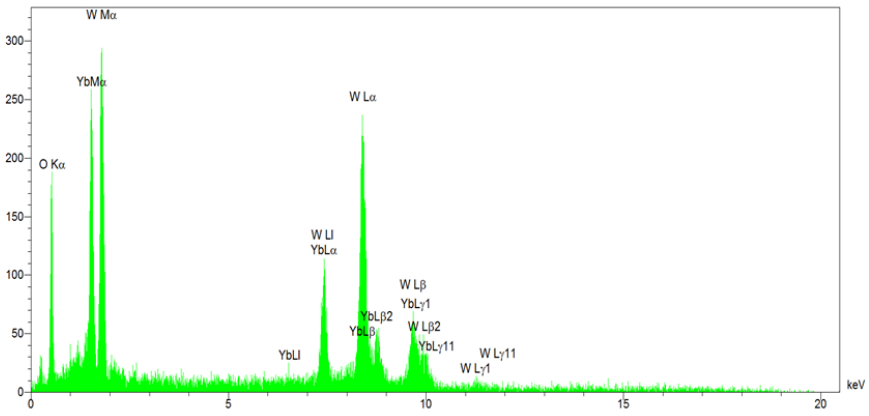

Fig. 4. EDAX spectrum of synthesized ytterbium tungstate nanoparticles by precipitation method

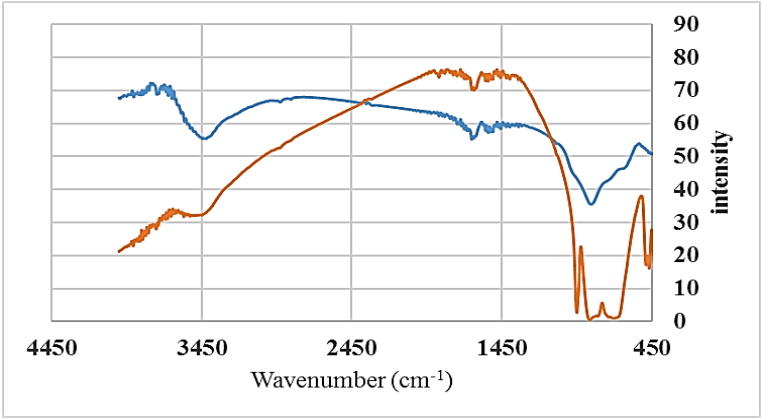

Fig. 5. FT-IR spectra for prepared ytterbium tungstate nanoparticles by precipitation reaction (a) before annealing, (b) after annealing at 750 °C

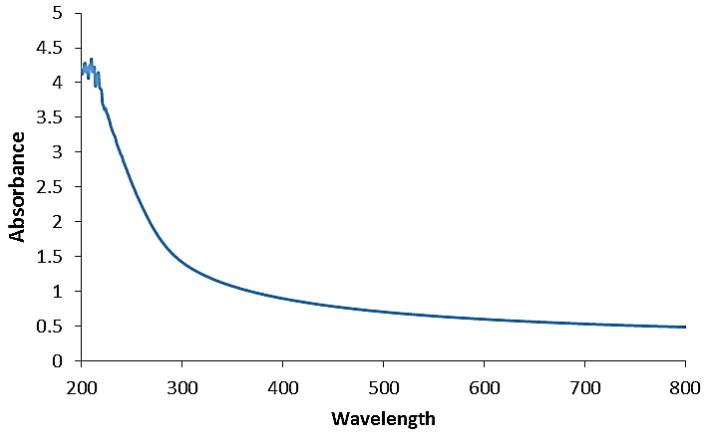

Fig. 6. UV-Vis absorption spectra of the ytterbium tungstate nanoparticles prepared via precipitation method under optimum conditions

3.2. BET analysis

Surface area and pore volume of ytterbium(III) tungstate nanoparticles have been determined using BET. Adsorption/desorption isotherm as well as BJH plot of the as prepared sample have been showed in Fig. 7a and b. Fig. 7b represents that the sample have a wide distribution of pores size with a maximum diameter of around 67.6 nm. The results shows that the specific surface areas, total pore volume and mean pore diameter of ytterbium(III) tungstate nanoparticles are 65.604 m^2/g, 0.3771 cm^3/g and 15.77 nm, respectively. The N_2 adsorption/desorption isotherm of the sample according to the IUPAC categorization fit with H1-type hysteresis loops which is the important attributes for ordered mesophorous compounds.

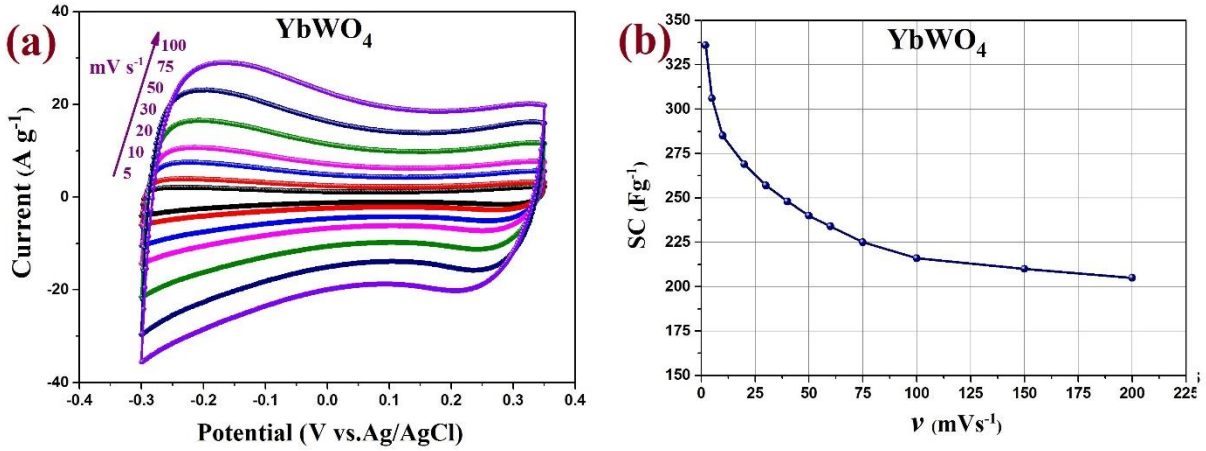

Fig. 7. (a) CVs of the ytterbium tungstate electrode at different scan rates of 5, 10, 20, 30, 50, 75 and 100 mV s^{-1} in a potential range of -0.3 to 0.35 V in 2.0 M H_2SO_4 aqueous electrolyte; (b) Specific capacitance as a function of the sweep rates for the ytterbium tungstate electrode

3.3. CV, SC values and CCV

Knowing that CV analyses can be a good source for information on the supercapacitive performance of electrocapacitor, different CV analyses were performed. Fig. 7a illustrates the CVs obtained using an ytterbium(III) tungstate electrode in the optimal potential range of -0.3 V to 0.35 V (*vs.* Ag/AgCl) at scan rates in the range of 5-100 mV s^{-1}. These approximate mirror-image peaks with regard to the zero-current line, show a fast current change upon voltage reversals (identical to the quasi-rectangular shapes and symmetric I-V responses), which indicates a perfect pseudo-capacitive behavior on the part of the electroactive materials.

Fig. 7b is a plot of SC values of the working electrode material against the scan rate. The plot shows a decrease in the SC value from 336 to 205 Fg^{-1} with increasing the scan rate from 2 to 200 mVs^{-1}. This can arise from the point that at lower scan rates the proton

ions present in the electrolyte find the required time to diffuse into the pores of the compound, which virtually increases the available surface of the material for effective redox reactions. However, this becomes inviable at high scan rates, where only the outer surface of the material is accessible to the ions in the short time frames available. It is hence clear that increasing the scan rate leads to lower total SC values.

CCV analyses, on the other hand, constitute a very powerful technique for studying the changes in the charge storage capability of a capacitor or electrode during and after numerous potential cycling [41-43]. Accordingly the effects of numerous potential cycles on the stability of the working electrode were evaluated. The plot of the SC value obtained for each CV against the number of cycles, is presented in Fig. 8a. Fig. 8b. Obviously, the SC of the electrode material did not get less than 95.8% of the initial value after 4000 scans at scan of 200 mVs^{-1}. This indicates that the electrode material is suitable for fast-charging applications. Fig. 8b shows the 3D CCVs obtained using $Yb_2(WO_4)_3$ based working electrode, in a 2.0 M H_2SO_4 solution at 200 mVs^{-1} in, which more markedly illustrates the changes in the CVs with the number of cycles.

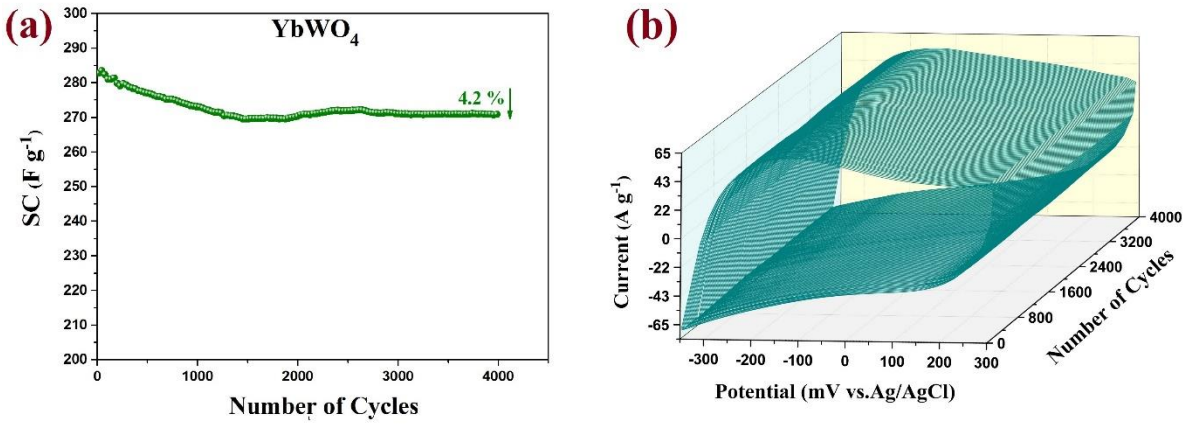

Fig. 8. (a) Variation of the specific capacitance of the ytterbium tungstate electrode as a function of number of cycles at 200 mVs^{-1}, and (ab) 3D-CCV curves of the ytterbium tungstate electrode measured at scan 200 mVs^{-1}

3.4. GCD experiments

Galvanostatic charge/discharge (GCD) analysis offers a powerful tool to compute the supercapacitive performance of an electrode which is subjected to controlled circumstances. The technique is performed using a three electrode. In the present work, the studies were conducted in potential range of -0.3 to 0.35 V, and the results (Fig. 9a), obtained at various current densities from 1 to 16 Ag^{-1}, are in the form of an equilateral triangle. This suggests the good reversibility and perfect capacitive behavior of the

electrode material during the charge/discharge processes [44]. The changes in the SC values as a function of current densities are plotted in Fig. 9b. One can see that only a 42.6% reduction happened in the SC values even at 32 Ag^{-1}, indicating the good capacitive retaining of the electroactive material under the test conditions. The SC values obtained through GCD were in good agreement with those based on the CV results. The power performance of the material was also studied making use of the power density against energy density or Ragone plots. The energy and power densities in Fig. 9c, were derived from GCD data obtained at different current densities. The maximum energy density, which was observed at a power density of 325 WKg^{-1}, was 17.5 $WhKg^{-1}$. This value is much bigger than those reported for similar electrodes in aqueous media [45-47]. Accordingly, nanostructured ytterbium(III) tungstate can be concluded as a good material for constructing electrodes to be used in supercapacitors.

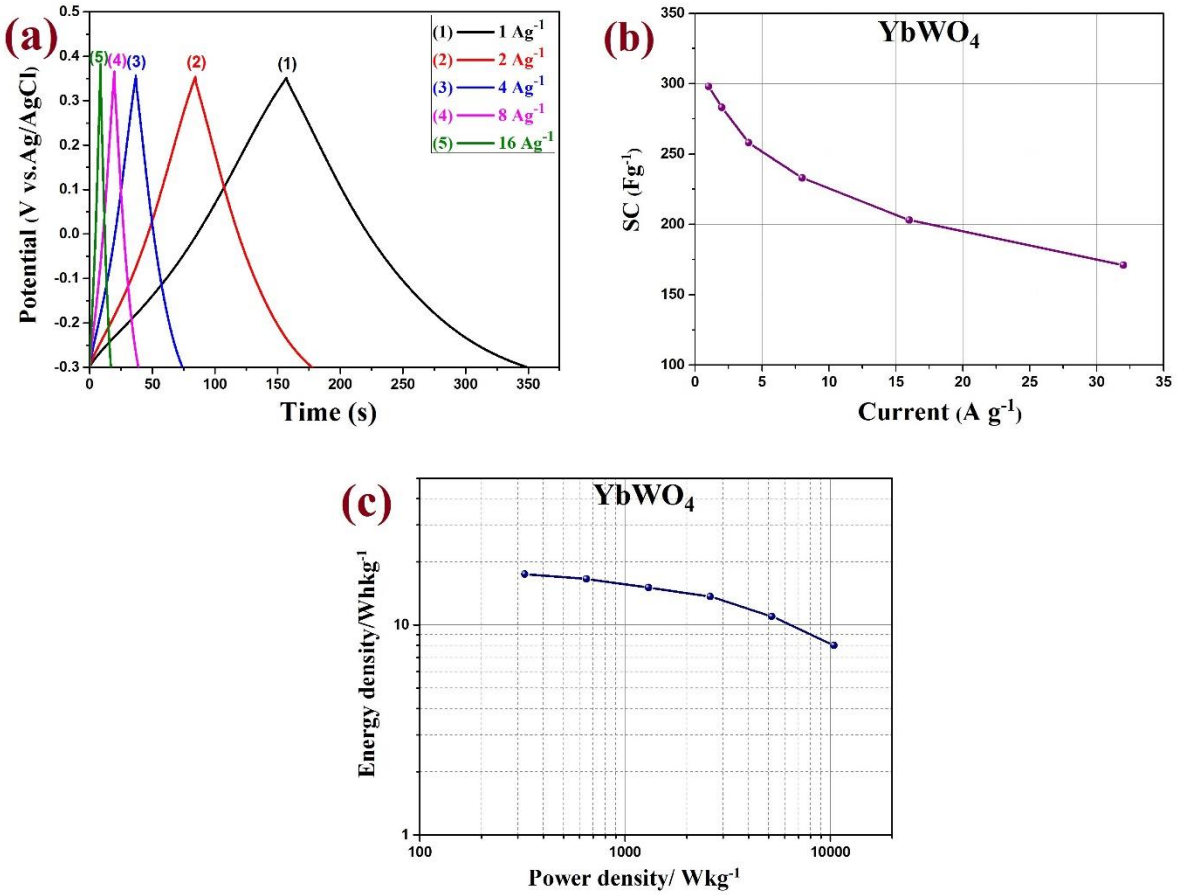

Fig. 9. (a) Charge/discharge curves of the ytterbium tungstate electrode at different current densities between 1 to 16 Ag^{-1} in 2.0 M H_2SO_4 aqueous electrolyte; (b) variation of SC at different current density for the $Yb_2(WO_4)_3$ electrode and (c) Ragone plots obtained for the $Yb_2(WO_4)_3$ electrode

In general, According to the electrochemical results, supercapacitive performance of $YbWO_4$ electrode is much better in comparison with other works that are listed in Table 1 [48].

Table 1. Comparison of supercapacitive behavior of between ytterbium tungstate electrode and some reported metal tungstate nanostructure electrodes

	Electrolyte	**Potential window (V)**	**Specific capacitance**	**Cycling stability**	**Ref.**
$SnWO_4$	3.0 M KOH	0.0 - 0.55	242 Fg^{-1} (5 mV s^{-1})	85% (4000 cycles)	[50]
$FeWO_4$	5 M $LiNO_3$	−0.6 - 0.0	35 Fg^{-1} (10 mV s^{-1})	93.0% (10000 cycles)	[51]
$MnWO_4$	0.1 M Na_2SO_4	0.0 - 1.0	34 Fg^{-1} (0.5 mA cm^{-2})	-	[52]
$NiWO_4$	2.0 M KOH	0.0 - 0.6	173 Fg^{-1} (5 mV s^{-1})	90% (1000 cycles)	[53]
$CuWO_4$	0.5 M HCl	-0.1 - 0.8	77 Fg^{-1} (5 mV s^{-1})	-	[54]
$CoWO_4$	2.0 M KOH	−0.25 - 0.45	60.6 Fg^{-1} (5 mV s^{-1})	94.7% (1000 cycles)	[55]
$SmWO_4$	2.0 M H_2SO_4	−0.8 - 0.2	321 Fg^{-1} (2 mV s^{-1})	99.0% (4000 cycles)	[32]
$YBWO_4$	2.0 M H_2SO_4	−0.8 - 0.2	336 Fg^{-1} (2 mV s^{-1})	95.8% (4000 cycles)	This Work

3.5. Electrochemical Impedance Spectroscopy (EIS)

EIS is a key method to compute the supercapacitive performance and typical resistance of materials. Fig. 10 illustrates the Nyquist plots of the ytterbium(III) tungstate-based electrodes at open circuit potentials (0.1–10^5 Hz). These plots are composed of a semicircular section in great frequencies and a straight part at lower frequencies. The equivalent circuit for the Nyquist graph (Fig. 10) includes R_s, R_{ct}, C_{dl}, $Z_{w,}$ and C_F, which respectively correspond to the solution and charge-transfer resistances, capacitance of the double layer, and Warburg impedance [49].

The R_s value calculated for the ytterbium(III) tungstate electrode was 0.25 Ω. R_{ct} or the electrode/electrolyte interfacial charge transfer resistance, determined based on the diameter of the semicircular section of the plots was 5.83 Ω. This low value indicates that the electrode/electrolyte interface facilitates the electrochemical reaction given the nature of the electroactive material used in the electrode.

The respective values for C_{dl} (the electrical double layer capacitance at the electrode/electrolyte interface) and C_F (the pseudocapacitance of the Faradic reaction)

[50] were 0.39 mF and 398 mF. Z_W or the Warburg resistance, which reflects the frequency dependency of ion diffusion/transport to the electrode surface [51] was almost ideal in the case of the $Yb_2(WO_4)_3$-based electrodes. This was reflected by the close to vertical line and complies with the CV and GCD data.

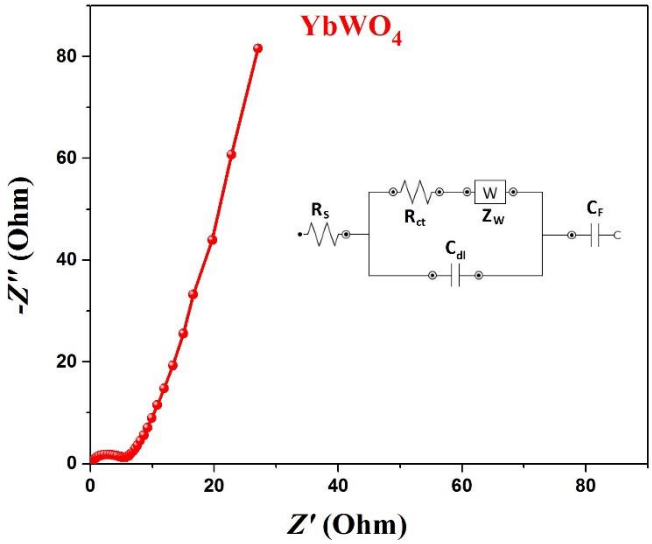

Fig. 10. Impedance spectra of the ytterbium tungstate electrode, measured at an AC amplitude of 10 mV, in 2.0 M H_2SO_4 aqueous electrolyte

4. CONCLUSION

In this report, ytterbium tungstate nanoparticles were prepared through a simple precipitation procedure. The shape and chemistry-based structure of the fabricated nanoparticles were studied using different instrumental techniques including SEM, TEM, XRD, EDS as well as FT-IR. Electrochemical evaluations indicated that electrodes, based on the prepared material, have a very good supercapacitive performance. Thus was reflected, in part, by the SC value of about 336 Fg^{-1} (at 2 mVs^{-1}). The durability of the properties of the electrodes were assessed through CCV tests at 200 mVs^{-1}, and the results proved that the SC of the electrodes did not get lower than about 95.8% of their beginning values, even after 4000 successive potential cycles. EIS and GCD experiments further supported the mentioned observations and, as a result, it was concluded that ytterbium(III) tungstate is a promising candidate for constructing efficient supercapacitor electrodes.

REFERENCE

[1] F. Gandomi, S. M. Peymani-Motlagh, M. Rostami, A. Sobhani-Nasab, M. Fasihi-Ramandi, M. Eghbali-Arani, R. Ahmadian, N. Gholipour, M.Rahimi-Nasrabadi, and M. R. Ganjali, J. Mater. Sci.: Mater. Electron. 30 (2019) 19691.

[2] M. A. Marsooli, M. Fasihi-Ramandi, K. Adib, S. Pourmasoud, F. Ahmadi, M. R. Ganjali, A. Sobhani Nasab, M. R. Nasrabadi, and M. E. Plonska-Brzezinska, Materials 12 (2019) 3274.

[3] A. Sobhani-Nasab, S. M. Hosseinpour-Mashkani, M .Salavati-Niasari, H. Taqriri, S. Bagheri, and K. Saberyan, J. Mater. Sci: Mater. Electron. 26 (2015) 5735.

[4] M. Salavati-Niasari, F. Soofivand, A. Sobhani-Nasab, M. Shakouri-Arani, M. Hamadanian, and S. Bagheri, J. Mater. Sci: Mater. Electron. 28 (2017)14965.

[5] S. S. Hosseinpour-Mashkani, and A. Sobhani-Nasab, J. Mater. Sci.: Mater. Electron. 28 (2017) 16459.

[6] M. Ramezani, A. Sobhani-Nasab, and S. M. Hosseinpour-Mashkani, J. Mater. Sci.: Mater. Electron. 26 (2015) 4848.

[7] S. M. Hosseinpour-Mashkani, A. Sobhani-Nasab, and M. Mehrzad, J. Mater. Sci.: Mater. Electron. 27 (2016) 5758.

[8] S. M. Hosseinpour-Mashkani, and A.Sobhani-Nasab, J. Mater. Sci.: Mater. Electron. 27 (2016) 7548.

[9] S. M. Hosseinpour-Mashkani, and A. Sobhani-Nasab, J. Mater. Sci.: Mater. Electron. 27 (2016) 3240.

[10] A. Sobhani-Nasab, and M. Behpour, J. Mater. Sci.: Mater. Electron. 27 (2016) 1191.

[11] S. S. Hosseinpour-Mashkani, S. S. Hosseinpour-Mashkani, and A. Sobhani-Nasab, J. Mater. Sci.: Mater. Electron. 27 (2016) 4351.

[12] M. Rahimi-Nasrabadi, A. Ghaderi, H. R. Banafshe, M. Eghbali-Arani, M. Akbari, F. Ahmadi, S. Pourmasoud, and A. Sobhani-Nasab, J. Mater. Sci.: Mater. Electron. 30 (2019) 15854.

[13] A. Sobhani-Nasab, S. Behvandi, M. A. Karimi, E. Sohouli, M. S. Karimi, N. Gholipour, F. Ahmadi. and M. Rahimi-Nasrabadi, Ceramics Int. 45 (2019) 17847.

[14] A. Sobhani-Nasab, M. Behpour, M. Rahimi-Nasrabadi, F. Ahmadi, S. Pourmasoud, and F. Sedighi, Ultrason. Sonochem. 50 (2019) 46.

[15] S. M. Peymani-Motlagh, A. Sobhani-Nasab, M. Rostami, H. Sobati, M. Eghbali-Arani, M. Fasihi-Ramandi, M. R. Ganjali, and M. Rahimi-Nasrabadi, J. Mater. Sci.: Mater. Electron. 30 (2019) 6902.

[16] A. Sobhani-Nasab, M. Behpour, M. Rahimi-Nasrabadi, F. Ahmadi, and S. Pourmasoud, J. Mater. Sci.: Mater. Electron. 30 (2019) 5854.

[17] H. Kooshki, A. Sobhani-Nasab, M. Eghbali-Arani, F. Ahmadi, V. Ameri, and M. Rahimi-Nasrabadi, Separat. Purif. Technol. 211 (2019) 873.

[18] S. M. Asgarian, S. Pourmasoud, Z. Kargar, A. Sobhani-Nasab, and M. Eghbali-Arani, Mater. Res. Express. 6 (2018) 015023.

[19] F. Sedighi, M. Esmaeili-Zare, A. Sobhani-Nasab, and M. Behpour, J. Mater. Sci.: Mater. Electron. 29 (2018) 13737.

[20] M. Eghbali-Arani, A. Sobhani-Nasab, M. Rahimi-Nasrabadi, and S. Pourmasoud, J. Electron. Mater. 47 (2018) 3757.
[21] A. Sobhani-Nasab, S. Pourmasoud, F. Ahmadi, M. Wysokowski, T. Jesionowski, H. Ehrlich, and M. Rahimi-Nasrabadi, Mater. Lett. 238 (2019) 159.
[22] A. M. Zardkhoshoui, and S. S. H. Davarani, J. Alloy. Compound. 769 (2018) 922.
[23] S. Faraji, and F. N. Ani, J. Power Sourc. 263 (2014) 338.
[24] A. Khoobi, F. Shahdost-fard, M. Arbabi, M. Akbari, H. Mirzaei, M. Nejati, M. Lotfinia, A. Sobhani-Nasab, and H. R. Banafshe, Polyhedron 177 (2020) 114302.
[25] M. Aghazadeh, I. Karimzadeh, and M. R. Ganjali, J. Mater. Sci.: Mater. Electron. 28 (2017) 13532.
[26] M. Aghazadeh, J. Mater. Sci.: Mater. Electron. 28 (2017) 3108.
[27] H. Heydari, S. E. Moosavifard, S. Elyasi, and M. Shahraki, Appl. Surf. Sci. 394 (2017) 425.
[28] O. Moradlou, H. Ansarinejad, M. Hosseinzadeh, and H. Kazemi, J. Alloy. Compound. 755 (2018) 231.
[29] M. Aghazadeh, R. Ahmadi, D. Gharailou, M. R. Ganjali, and P. Norouzi, J. Mater. Sci.: Mater. Electron. 27 (2016) 8623.
[30] D. P. Ojha, H. P. Karki, J. hee Song, and H. J. Kim, Chem. Phys. Lett. 712 (2018) 83.
[31] S. Yao, L. Xing, Y. Dong, and X. Wu, J. Coll. Interf. Sci. 531 (2018) 216.
[32] M. Rahimi-Nasrabadi, M. Behpour, A. Sobhani-Nasab, and S. M. Hosseinpour-Mashkani, J. Mater. Sci.: Mater. Electron. 26 (2015) 9776.
[33] M. Rahimi-Nasrabadi, M. Behpour, A. Sobhani-Nasab, and M. R. Jeddy, J. Mater. Sci.: Mater. Electron. 27 (2016) 11691.
[34] M. Rostami, M. Rahimi-Nasrabadi, M. R. Ganjali, F. Ahmadi, A. F. Shojaei, and M. D. Rafiee, J. Mater. Sci. 52 (2017) 7008.
[35] M. Rahimi-Nasrabadi, S. M. Pourmortazavi, M. Aghazadeh, M. R. Ganjali, M. S. Karimi, and P. Novrouzi, J. Mater. Sci.: Mater. Electron. 28 (2017) 3780.
[36] M. Rahimi-Nasrabadi, S. M. Pourmortazavi, M. R. Ganjali, P. Norouzi, F. Faridbod, and M. S. Karimi, J. Mater. Sci.: Mater. Electron. 27 (2016) 12860.
[37] S. Devaraj, and N. Munichandraiah, Electrochem. Solid-State Lett. 8 (2005) A373-A7.
[38] S. M. Pourmortazavi, M. Taghdiri, N. Samimi, and M. Rahimi-Nasrabadi, Mater. Lett. 121 (2014) 5.
[39] A. Sobhani-Nasab, M. Rahimi-Nasrabadi, H. R. Naderi, V. Pourmohamadian, F. Ahmadi, M. R. Ganjali, and H. Ehrlich, Ultrason. Sonochem. 45 (2018) 189.
[40] A. Sobhani-Nasab, H. Naderi, M. Rahimi-Nasrabadi, and M. R. Ganjali, J. Mater. Sci.: Mater. Electron. 28 (2017) 8588.
[41] S. Gholamrezaei, and M. Salavati-Niasari, J. Mol. Liquid. 243 (2017) 227.

[42] A. Hosseini, E. Sohouli, M. Gholami, A. Sobhani-Nasab, and S. A. Mirhosseini, Anal. Bioanal. Electrochem. 11 (2019) 996.
[43] A. Khoshroo, L. Hosseinzadeh, A. Sobhani-Nasab, M. Rahimi-Nasrabadi, and H. Ehrlich, J. Electroanal. Chem. 823 (2018) 61.
[44] M. Aghazadeh, and M. R. Ganjali, J. Mate. Sci.: Mater. Electron. 28 (2017) 11406.
[45] B. Li, Y. Fu, H. Xia, and X. Wang, Mater. Lett.. 122 (2014) 193.
[46] X. Zhang, X. Sun, H. Zhang, D. Zhang, and Y. Ma, Mater. Chem. Phys. 137 (2012) 290.
[47] G. Yu, L. Hu, M. Vosgueritchian, H. Wang, X. Xie, J. R. McDonough, X. Cui, Y. Cui, and Z. Bao, Nano Lett. 11 (2011) 2905.
[48] S. R. Ede, and S. Kundu, ACS Sustainable Chem. Eng. 3 (2015) 2321.
[49] M. Aghazadeh, I. Karimzadeh, and M. R. Ganjali, J. Electron. Mater. 47 (2018) 3026.
[50] M. Aghazadeh, M. G. Maragheh, M. R. Ganjali, P. Norouzi, and F. Faridbod, Appl. Surf. Sci. 364 (2016) 141.
[51] K. Zhang, L. L. Zhang, X. Zhao, and J. Wu, Chem. Mater. 22 (2010) 1392.
[52] U. Nithiyanantham, S. R. Ede, T. Kesavan, P. Ragupathy, M. D. Mukadam, S. M. Yusuf, and S. Kundu, RSC Adv. 4 (2014) 38169.
[53] S.R. Ede, S. Anantharaj, and S. Kundu, Cryst. Growth Des. 15 (2015) 673.
[54] R.D. Kumar, and S. Karuppuchamy, Ceram. Int. 40 (2014) 12397.
[55] X. Xu, J. Shen, N. Li, and M. Ye, Electrochim. Acta 150 (2013) 23.